AGU PUBLICATIONS

JGR

Journal of Geophysical Research: Space Physics

RESEARCH ARTICLE
10.1002/2016JA022409

Key Points:
- First multispacecraft analysis of magnetic field curvature in the ion diffusion region
- Electron dynamics is analyzed as a function of magnetic field curvature
- Observational evidence for magnetic curvature-induced electron pitch angle scattering

Correspondence to:
Y. C. Zhang,
zyc@nssc.ac.cn

Citation:
Zhang, Y. C., et al. (2016), First in situ evidence of electron pitch angle scattering due to magnetic field line curvature in the Ion diffusion region, *J. Geophys. Res. Space Physics*, *121*, 4103–4110, doi:10.1002/2016JA022409.

Received 21 JAN 2016
Accepted 13 APR 2016
Accepted article online 28 APR 2016
Published online 7 MAY 2016

First in situ evidence of electron pitch angle scattering due to magnetic field line curvature in the Ion diffusion region

Y. C. Zhang[1,2,3,4], C. Shen[5], A. Marchaudon[3,4], Z. J. Rong[2], B. Lavraud[3,4], A. Fazakerley[6], Z. Yao[6], B. Mihaljcic[6], Y. Ji[7], Y. H. Ma[5], and Z. X. Liu[1]

[1]State Key Laboratory of Space Weather, National Space Science Center, Chinese Academy of Sciences, Beijing, China, [2]Key Laboratory of Earth and Planetary Physics, Institute of Geology and Geophysics, Chinese Academy of Sciences, Beijing, China, [3]Institut de Recherche and Astrophysique et Planétologie, Université de Toulouse (UPS), Toulouse, France, [4]Centre National de la Recherche Scientifique, UMR 5277, Toulouse, France, [5]Shenzhen Graduate School, Harbin Institute of Technology, Shenzhen, China, [6]Mullard Space Science Laboratory, University College London, London, UK, [7]State Key Laboratory for Turbulence & Complex Systems, Peking University, Beijing, China

Abstract Theory predicts that the first adiabatic invariant of a charged particle may be violated in a region of highly curved field lines, leading to significant pitch angle scattering for particles whose gyroradius are comparable to the radius of the magnetic field line curvature. This scattering generates more isotropic particle distribution functions, with important impacts on the presence or absence of plasma instabilities. Using magnetic curvature analysis based on multipoint Cluster spacecraft observations, we present the first investigation of magnetic curvature in the vicinity of an ion diffusion region where reconnected field lines are highly curved. Electrons at energies > 8 keV show a clear pitch angle ordering between bidirectional and trapped distribution in surrounding regions, while we show that in the more central part of the ion diffusion region electrons above such energies become isotropic. By contrast, colder electrons (~1 keV) retain their bidirectional character throughout the diffusion regions. The calculated adiabatic parameter K^2 for these electrons is in agreement with theory. This study provides the first observational evidence for particle pitch angle scattering due to magnetic field lines with well characterized curvature in a space plasma.

1. Introduction

In magnetized plasma environments, such as the Earth's magnetosphere, charged particles experience three types of regular motions: gyro-motion around magnetic field lines, bounce between magnetic mirrors, and drift across magnetic field lines. These regular motions can be described by adiabatic invariants [*Northrop*, 1963]. Under special conditions, these adiabatic invariants may be violated [*Chen*, 1992]. For instance, at the smallest scale the gyro-motion may be violated in a region of highly curved magnetic field lines; this occurs when the curvature radius of the magnetic field lines becomes comparable to the particle gyroradius, leading to significant particle scattering as expected by theory [*Büchner and Zelenyi*, 1989; *Young et al*., 2008]. The scattering should be triggered by the resonance between Larmor rotation and higher harmonics of the bounce motion when the resonance condition satisfies a threshold $< \Omega_L > = n \cdot \omega_b$ where n is a positive integer and Ω_L is the Larmor frequency averaged over the bounce period $T_b = 2\pi/\omega_b$. Theory shows that as the calculation of ω_b is strongly related to the curvature radius R_c, eventually the resonance threshold is governed by an adiabatic parameter $K^2 = R_c/R_g$,where R_g is the particle gyroradius [*Büchner and Zelenyi*, 1989]. In the Earth's magnetosphere, K^2 values in most magnetic configurations are so high that essentially all the particles, and electrons in particular, are always tied to magnetic field lines. As K^2 decreases below the threshold value of 25, theory and modeling [*Büchner and Zelenyi*, 1989; *Young et al*., 2008] show that curvature pitch angle scattering is triggered, so that any anisotropic particle distribution rapidly becomes isotropic or chaotic. Particle behavior is totally chaotic when K^2 drops below 10 [*Sergeev et al*., 1983]. The resulting untied particles can contribute to plasma instabilities which play a key role in plasma processes such as the onset of magnetic reconnection [*Bessho and Bhattacharjee*, 2005] and magnetospheric substorms [*Baker et al*., 1986]. Magnetic curvature pitch angle scattering theory has been used to interpret the behavior of proton dynamics in the radiation belt and ring current [*Zou et al*., 2011; *Shen et al*., 2014]. In the diffusion region of magnetic reconnection, modeling works have shown that accelerated electrons become more chaotic as they approach the X line [*Wang et al*., 2010; *Bessho et al*., 2015], where the curvature radius of magnetic field lines becomes comparable to the electron gyroradius. This curvature radius is expected to become even smaller in the diffusion

region for antiparallel fields than for significant guide field conditions. Isotropic electron distributions have also been observed in the diffusion region. These observations were explained by magnetic curvature pitch angle scattering, based on the comparison between the electron gyroradius and the scale (half width) of the current sheet [*Wang et al*., 2010]. These works, however, only used proxies for the magnetic field curvature radius. Until now, there remains a lack of observational evidence for this theory, because it is not easy to derive precise K^2 from observations without a precise determination of the curvature radius of magnetic field lines.

In this paper, by applying magnetic curvature analysis (MCA) method [*Shen et al*., 2003] to a unique magnetic reconnection event observed by Cluster, we investigate for the first time the magnetic curvature radius in the ion diffusion region. The adiabatic parameter K^2 is calculated for electrons based on magnetic curvature radius and is discussed together with electron distribution characteristics, in a comparison to theoretical predictions.

2. Observations

During the interval 23:28:00–23:33:00 UT on 19 September 2003 Cluster is located in the magnetotail at about [−17.45, 3.63, 0.52] R_E (GSM, geocentric solar magnetospheric coordinate system) with a minimum interspacecraft separation of ~160 km. This separation is much smaller than the scale of the ion diffusion region, which is controlled by the ion inertial length [*Ma and Bhattacharjee*, 2001; *Wang et al*., 2001; *Xiao et al*., 2007], which is here of order up to ~1000 km. The magnetic field data from the Flux Gate Magnetometer (FGM) [*Balogh et al*., 2001], ion data from the Cluster Ion Spectrometer (CIS) experiment [*Rème et al*., 2001], and electron data from the Plasma Electron And Current Experiment (PEACE) [*Johnstone et al*., 1997] are used in this study (from the Cluster Science Archive) [*Laakso et al*., 2010]. To best investigate electron dynamics, we present the reduced 3-D electron distribution with subspin resolution from High Energy Electron Analyser (HEEA) of PEACE instrument [*Fazakerley et al*., 2010]. During this short interval, the reduced 3-D distribution was available continuously only from Cluster-2 (C2). There is no ion data available from C2, however, so ion data from Cluster-3 (C3) is used for context. This assumption is acceptable since the interspacecraft separation is smaller than lthe ion inertial scale. Figure 1 displays Cluster observations during this time interval in GSM coordinates. The red labels P1, P2, P3, and P4 at the top of Figure 1 refer to the red phases P1, P2, P3, and P4 from the schematic of the Cluster trajectory in Figure 2.

Figures 1a–1c show the magnetic field components [*Bx*, *By*, *Bz*] from the four Cluster spacecraft. At 23:28:00 UT, Cluster is in the northern plasma sheet, where *Bx* is stable and positive with large values compared to later time. At 23:28:20 UT, marked with the first vertical dashed line in Figure 1, *Bx* drops and a tailward increase in *Vx* is observed; meanwhile, the amplitudes of the negative *By* and *Bz* components begin to increase. These observations imply that Cluster crosses the separatrix and enters the upper right quadrant of the ion diffusion region (red phase P1 in Figure 2), where the increase in *By* corresponds to the Hall field signature. The electric field observations (not shown here) in this case agree well with the presence of Hall electric field [*Borg et al*., 2005], which implies that ions are not frozen-in as expected for the observation of an ion diffusion region [*Eastwood et al*., 2007; *Paschmann*, 2008]. At 23:29:44 UT, marked with the second vertical dashed line, Cluster observes a change from a tailward flow to an Earthward flow (Figure 1d). This flow reversal is concomitant with a change from a southward to northward *Bz*, while *Bx* stays positive. Such a feature indicates a crossing nearby the magnetotail reconnection line, with the spacecraft crossing from its tailward side to its Earthward side [*Borg et al*., 2005]. Cluster enters the upper left quadrant of the reconnection region at this time (the red phase P2 in Figure 2) and stays in its left-half branch (the red phase P4 in Figure 2) except for a short dip into a $Bz < 0$ region consistent with moving into the upper right quadrant (the red phase P3 in Figure 2) between 23:30:04 UT (as marked by the third vertical dashed line) and 23:30:16 UT (marked by the forth vertical dashed line). We performed the timing analysis on $Bz = 0$ crossings [*Schwartz*, 1998] around 23:30:07 UT and 23:30:18 UT and determined the direction of X line motion to be [0.93, −0.29, −0.23] and [−0.90, 0.41, 0.15] GSM, respectively. This means the X line is moving earthward first and then tailward, so Cluster crosses from P2 to P3 and then from P3 to P4. Near 23:30:16 UT, the magnetic field observed by Cluster-4 (C4) is different from the other three spacecraft, showing a tailward *Bx* at C4, but Earthward *Bx* at the other spacecraft, consistent with a short excursion into the southern magnetotail lobe. We note that this only affects the local magnetic field curvature calculation at this particular time. At

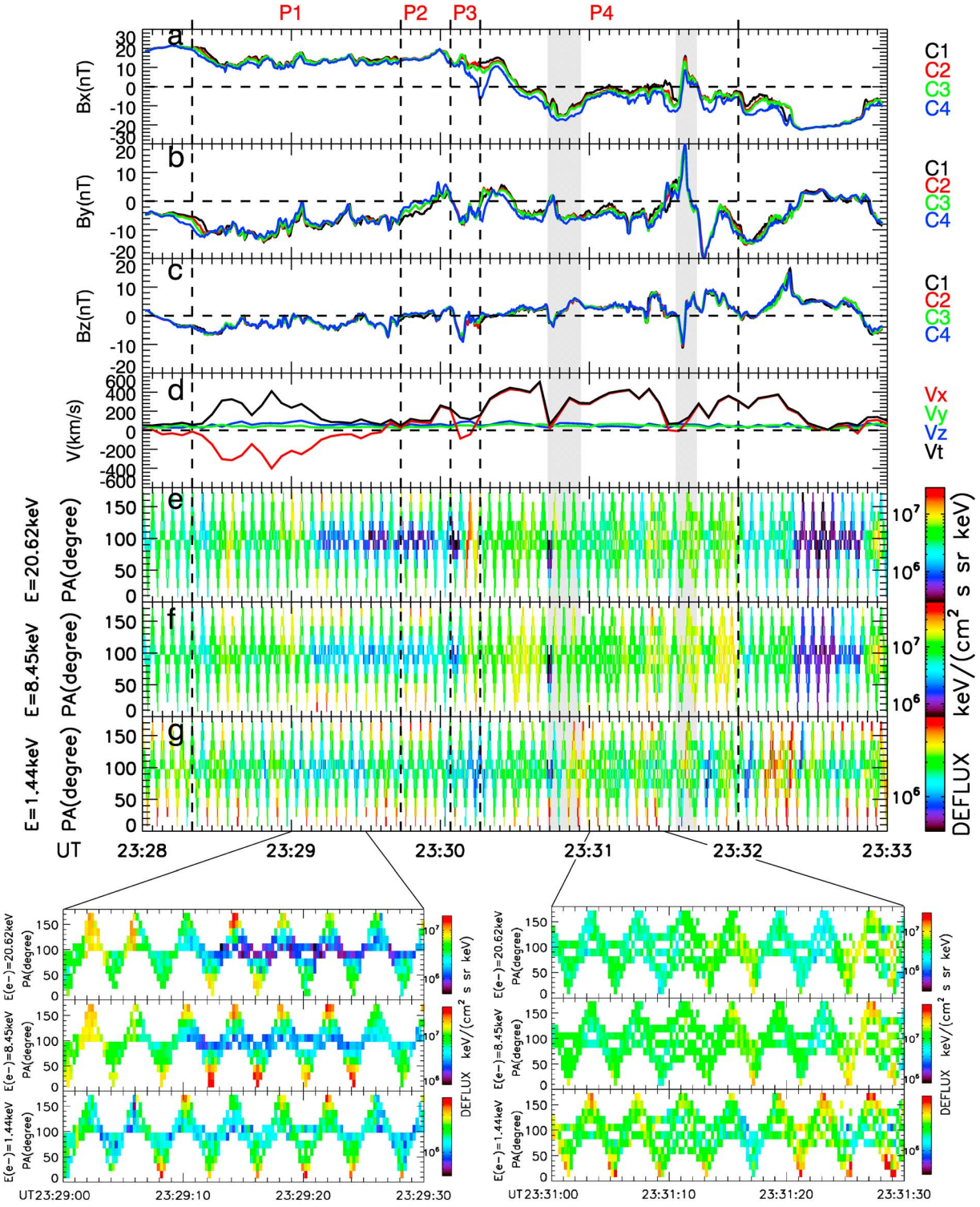

Figure 1. Cluster observations in the reconnection diffusion region on 19 September 2003. (a) *Bx*, (b) *By*, and (c) *Bz* from the four Cluster spacecraft; (d) ion velocity from C3; (e–g) electron pitch angle distributions at three energies from C2. Two panels at the bottom show the zoomed-in electron pitch angle spectra at three energies: during 23:29:00 UT–23:29:30 UT in Hall region on the left-hand side and during 23:31:00 UT–23:31:30 UT in inner outflow region on the right-hand side. The regions labeled P1, P2, P3, and P4 at the top correspond to phases P1, P2, P3, and P4 of the Cluster trajectory in Figure 2. The small-scale wave shape structuring in electron pitch angle distributions is due to the variable orientation of the pitch angle of a given PEACE instrument anode during the spacecraft spin.

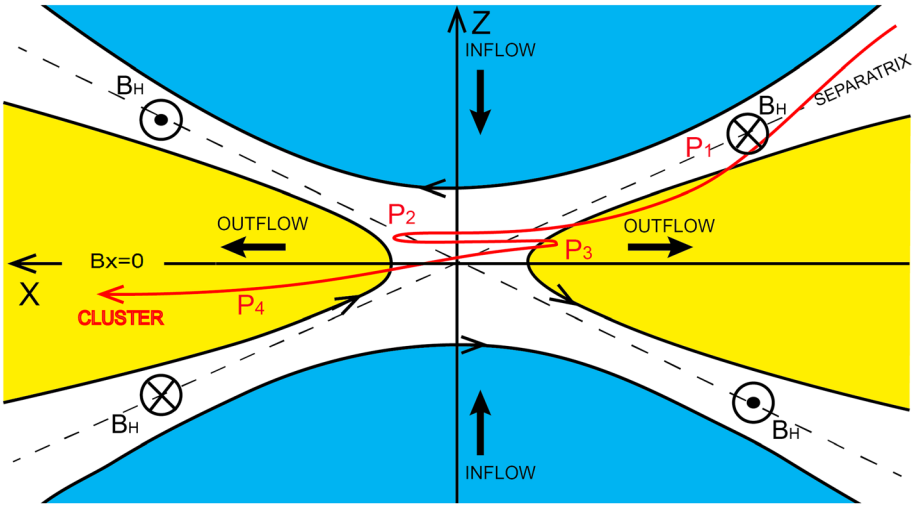

Figure 2. Sketch depicting the relative motion of the Cluster spacecraft in the vicinity of the ion diffusion region (with Hall magnetic field) during this event. The red phases P1, P2, P3, and P4 indicate the traversal of different parts of the ion diffusion region.

23:30:28 UT, *Bx* changes sign (becomes tailward), which implies that Cluster crosses the *Bx* = 0 symmetry line and enters the southern lobe region in the bottom left quadrant of the ion diffusion region. Cluster mainly stays in this quadrant for the rest of the time. Compared to the values in the Hall region in phase P1, *Bx* shows a lower magnitude and the magnitude of *By* also decreases in phases P3 and P4. This indicates that after 23:30:04 UT, Cluster is mainly meandering in the inner part of the outflow region between the north and south Hall regions. As this inner part is closer to *Bx* = 0 than where the Hall *By* peak is observed, we refer it as the inner outflow region. It should be noted that two south-north *Bz* bipolar signatures are observed in phase P4 (indicated by the gray shading in Figure 1). In these *Bz* bipolar signatures, the magnitude of south *Bz* increased to the maximum first and then decreases to zero. After the zero point of *Bz*, *Bz* turned northward and increased its magnitude to the maximum. North *Bz* completed the bipolar signature by decreasing its magnitude. For the first *Bz* bipolar signature, the magnitude of south *Bz* began to increase at 23:30:43 UT and north *Bz* ended the decrease of its magnitude at 23:30:55 UT. For the second *Bz* bipolar signature, the magnitude of south *Bz* began the increase at 23:31:35 UT and the magnitude of north *Bz* end the decrease at 23:31:43 UT. These are identified as two earthward moving magnetic flux ropes by *Huang et al*. [2010]. The *By* component in the plasma sheet adjacent to the reconnection region is only 5% of the total magnetic intensity, implying that this case can be classified as antiparallel reconnection [*Dunlop et al*., 2009].

Electrons at different energies display distinct behaviors in the Hall region (P1) and the inner outflow region (P4). Electron pitch angle distributions from C2 for three energies centered on 1.44 keV, 8.45 keV, and 20.62 keV are selected to show these behaviors in Figures 1e–1g: electrons with lower energy at 1.44 keV (Figure 1g) are bidirectional (enhanced fluxes in the field-aligned and antifield-aligned directions) for the whole crossing. For electrons with energies 8.45 keV and above (Figures 1e and 1f), the situation is more complex: in the end of phase P1, these electrons have the same anisotropic distribution as the lower energy electrons, while in phase P4, the electrons clearly display more isotropic distributions (between 23:30:16 UT and 23:32:00 UT marked by the fifth vertical dashed line in Figure 1). The spin-resolution 2-D electron pitch angle observations of Cluster-1 (C1), C3, and C4 display similar properties. To further illustrate the electrons' behavior, two panels at the bottom of Figure 1 provides the zoomed-in electron pitch angle distributions during two selected time intervals: 23:29:00 UT–23:29:30 UT in the Hall region on the left-hand side panel and 23:31:00 UT–23:31:30 UT in the inner outflow region on the right-hand side panel. As can be seen in the left panel, the fluxes of electrons at 8.45 keV and 20.62 keV sharply decrease at 90° pitch angle in the Hall region. By contrast, in the inner outflow region (right panel), electron fluxes at these energies increased in the perpendicular direction and decreased in the field-aligned direction, so that the electron distribution is nearly isotropic. At lower energies (1.44 keV) electron fluxes are depleted at 90° pitch angle and appear

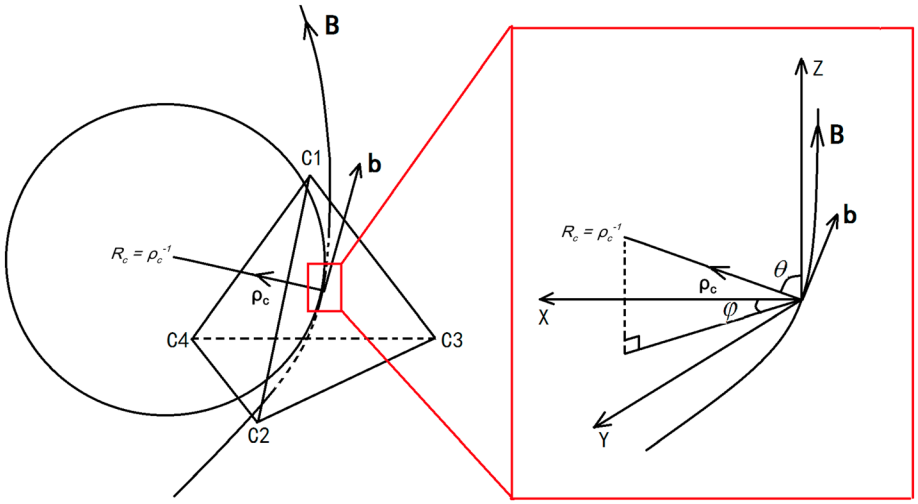

Figure 3. Sketch of how the four Cluster spacecraft (C1, C2, C3, and C4) measure the curvature radius (R_c) of magnetic field lines (B). b is the unit magnetic vector at the centroid of the Cluster tetrahedron; *X*, *Y*, and *Z* are the axes of the position coordinates describing the Cluster spacecraft locations (GSM); ϕ is the azimuthal angle of $\mathbf{P_c}$; θ is the elevation angle of $\mathbf{P_c}$.

bidirectional (anisotropic) in both the Hall and the inner outflow regions. The more global view obtained from electron pitch angle distributions at all energy bands, and at all spacecraft, supports these features (not shown).

In summary, during this event the spatial scale of the Cluster tetrahedron is sufficiently small (with a maximum value of 200 km) to ensure that all four spacecraft generally cross the same part of the diffusion region at most of the times. All four spacecraft indeed show similar magnetic field behavior, as observed in Figures 1a–1c. The Cluster spacecraft stay in the vicinity of the ion diffusion region during a 4 min interval, which ensures sufficient data coverage to get reliable results for the analysis of microscale kinetic process [*Chaston et al.*, 2009; *Zhou et al.*, 2009]. Electrons with high energies (8 keV and above) are highly isotropic in the inner outflow region, while they are not isotropic elsewhere such as the Hall region. By contrast also, electrons with lower energies remain magnetized during most of the whole interval, showing bidirectional structure in their pitch angle distributions.

3. Methods

The key idea of the magnetic curvature analysis (MCA) method as shown schematically in Figure 3 is to calculate the gradient of the magnetic unit vector b = B/|B|at the centroid of the Cluster tetrahedron using four individual magnetic field measurements. With this method we can determine the rotation rate of the magnetic field direction **b** along the magnetic field line, i.e., $b\cdot(\nabla\mathbf{b})$, which is just the curvature vector of the magnetic field line ($\mathbf{P_c}$). Furthermore, the scalar value of the curvature radius, $R_c = \rho_c^{-1}$, can be evaluated as shown in Figure 3. Combining the measured **b** and the calculated $\mathbf{P_c}$ (R_c), the geometrical configuration of the magnetic field lines can be revealed. The validity of the MCA method has been verified through application to mesoscale and microscale structures such as current sheets and plasmoids [*Shen et al.*, 2008; *Rong et al.*, 2011; *Zhang et al.*, 2013; *Yang et al.*, 2014], as well as on larger scale structures such as the ring current [*Shen et al.*, 2014]. The relative error for this method generally orders with $O \sim L/D$, and if the magnetic field is linearly varying in space within magnetic structure, the relative error will be at the second order, i.e., $O \sim (L/D)^2$, where *L* is the size of the Cluster tetrahedron and *D* is the typical spatial transverse scale of the magnetic structure [*Shen et al.*, 2003, 2007].

4. Discussion

Figures 4a and 4b show the variation of the direction (ϕ, θ) of P_c and curvature radius (R_c) versus time in GSM coordinates. θ ($0° \le \theta \le 180°$) is the elevation angle with 0° in positive GSM-Z and ϕ ($0° \le \phi \le 360°$) is the azimuthal angle with 0° in positive GSM-X and 90° along positive GSM-Y. We can see that in the branch of

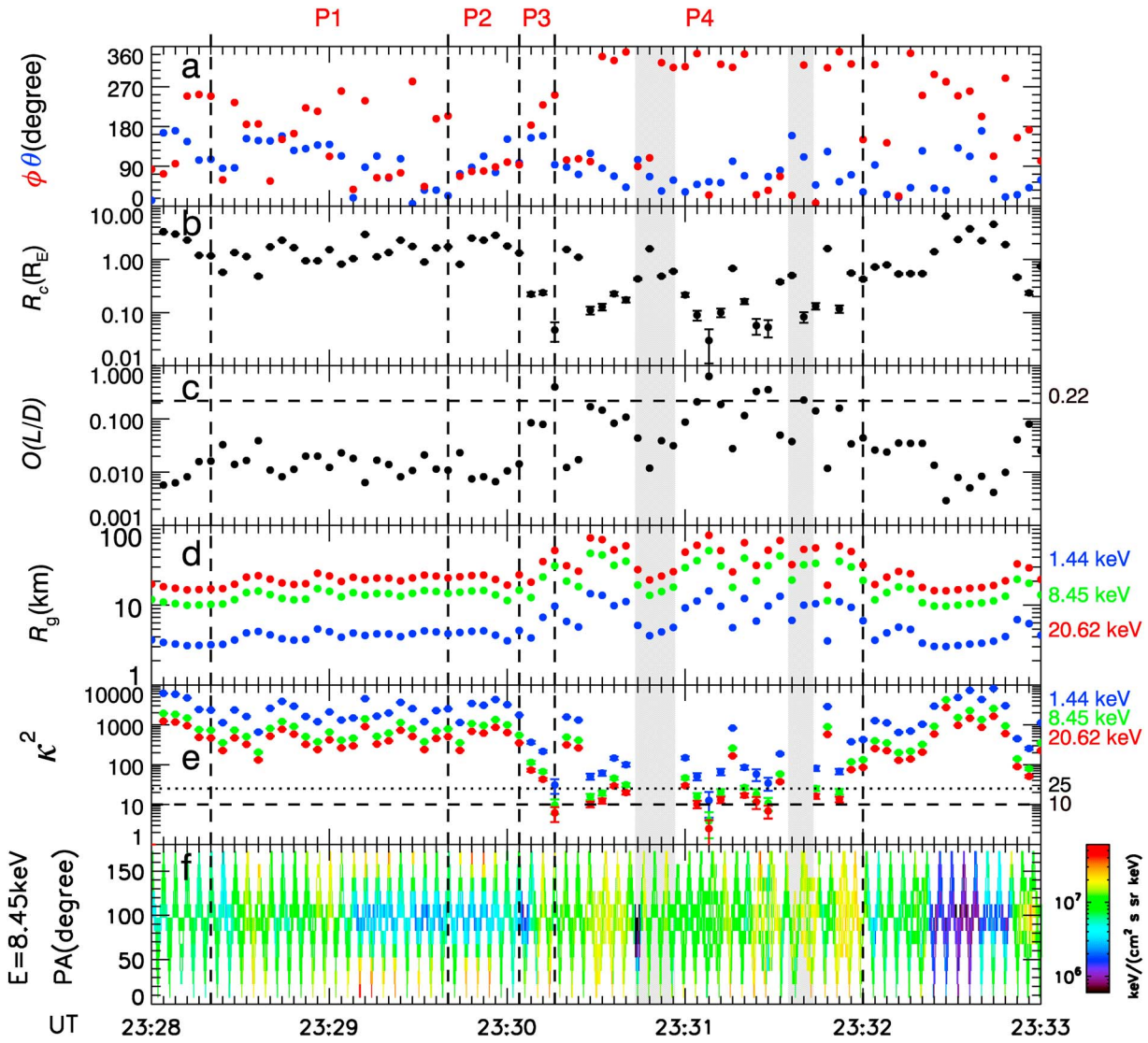

Figure 4. Results of magnetic curvature analysis in the diffusion region. (a) Direction of curvature of $\mathbf{P_c}$; (b) curvature radius of magnetic field lines; (c) error estimation for curvature calculation; (d) gyroradius of electrons at three energies; (e) adiabatic parameter K^2 of electrons at three energies; (f) Electron pitch angle distributions at 8.45 keV. The horizontal dashed line in Figure 4c indicates the value of 0.22 for the relative errors. To easily locate the data points on the vertical axes, each tick interval on the vertical axes in Figures 4b–4e is divided into nine minor intervals. The horizontal dotted and dashed lines in Figure 4e indicate $K^2 = 25$ and $K^2 = 10$, respectively. The red labels P1, P2, P3, and P4 at the top correspond to the colored phases P1, P2, P3, and P4 of the Cluster trajectory in Figure 2.

the Hall region marked as P1 at the top of Figure 4, the curvature radius R_c greatly fluctuates with values between 0.6 R_E and 4 R_E, and the P_c direction is not well organized, with pronounced deviations out of the plane to azimuth angles $\phi \sim 0°$ or 180°. In the Hall region, *By* Hall fields are comparable to the *Bx* component and contribute equally to R_c. Small temporal and spatial fluctuations in the Hall fields can be expected and can lead to some disorder in R_c, as observed in this case. Contrary to the situation in the Hall region, the curvature displays a more ordered behavior in the inner outflow region (P3 and P4): (1) R_c has values of no more than 1 R_E; (2) the directions of all $\mathbf{P_c}$ nearly lie in the day-night meridian plane; they are directed toward the Northern Hemisphere ($\phi \sim 360°$ or 0°, $\theta \sim$ around 60°) earthward of the X line (P4 region) and toward the Southern Hemisphere ($\phi \sim$ around 180°, $\theta \sim$150°) in the tailward (P3) region; and (3) the temporal variation of R_c is smooth. It can be inferred that magnetic field there displays a rather stable hyperbolic and nearly coplanar configuration, which supports antiparallel reconnection. It is striking that the value of the curvature radius is really small in the inner outflow region, marked as P4 in Figure 4, except for a few high values during the passage of the two magnetic flux ropes (indicated by the gray shading in Figure 4) due to their strong

core magnetic fields [*Zhang et al*., 2013]. The minimum value reaches 0.03 R_E (190 km) at 23:31:08 UT, which is comparable to the electron gyroradius. As shown in Figure 4d, the electron gyroradius typically range from a few kilometers to tens of kilometers, being a function of energy. From the theory described previously [*Chen*, 1992], the very small R_c will favor the initiation of curvature pitch angle scattering through reduction of adiabatic parameter K^2 below a specific threshold. Figure 4f again shows the C2 pitch angle distribution for higher energy electrons (8.45 keV). The most isotropic electrons distributions are clearly observed in this inner outflow region with low magnetic curvature radius.

To further quantify the electron dynamics, the adiabatic parameter K^2 for the three energies 1.44 keV, 8.45 keV, and 20.62 keV is calculated and displayed in Figure 4e. In Figure 4e, the K^2 threshold values of 25 and 10 for the onset of curvature pitch angle scattering and total chaos are indicated by the horizontal dotted line and the horizontal dashed line, respectively. To clearly see the K^2 distribution in the inner outflow region, the data points for K^2 in the two magnetic flux ropes have been removed. We can see that the K^2 values for the lower energy electrons (blue dots) lie above the horizontal dotted line, i.e., they are much higher than the threshold of 25 for the onset of curvature pitch angle scattering. The behavior of electrons at this energy is not affected by the highly curved reconnected magnetic field line. Electrons remain fully tied to the magnetic field, consistent with mostly bidirectional electron pitch angles essentially through the event. However, K^2 values for higher energy electrons (red and green dots) in the inner outflow region labeled as P4 clearly fall below the horizontal dotted line. It is thus reasonable to attribute the observed transition from anisotropic to isotropic distributions, for higher energy electrons, to the magnetic curvature pitch angle scattering [*Chen*, 1992; *Büchner and Zelenyi*, 1989; *Sergeev et al*., 1983].

As it is not known if the magnetic field variations in the diffusion region are linear or not, the first order of L/D is used for the relative error in the curvature calculation presented here. Figure 4c presents the estimation of the relative error $O(L/D)$. Here L is the scale of Cluster spacecraft separation ranging between 160 km and 200 km. The scale D of the physical structure being studied with the method is taken as the locally estimated curvature radius. The obtained relative errors are always below 22% except for a few points in the inner outflow region due to extremely low curvature radius. These errors are also provided in the estimates of K^2 in Figure 4e, where we can see that the errors overall do not significantly affect our result despite being in the limit of applicability of the method with magnetic curvature radius approaching the spacecraft separation.

5. Conclusions

In summary, owing to the localized topological changes associated with magnetic reconnection, the vicinity of the diffusion region provides an ideal location to check magnetic curvature pitch angle scattering theory. The configuration of the multisatellite Cluster mission and the application of the MCA method make this testing possible. We present the first such investigation of magnetic curvature in the vicinity of an ion diffusion region for a nearly antiparallel reconnection event in the Earth's magnetotail. The small Cluster interspacecraft separation (160–200 km) and relatively long duration within the inner outflow region make this event particularly appropriate for such investigation. We show that the magnetic field lines in the inner outflow region have a very small curvature radius, comparable to suprathermal electron gyroradii, thereby enabling the adiabatic parameter K^2 for electrons with energies ~8 keV and above to fall below the threshold for curvature pitch angle scattering. Following curvature pitch angle scattering, these electrons in the inner outflow region become highly isotropic, while in other regions and at lower energies electrons typically remains fully magnetized with either trapped or bidirectional pitch angle distributions. Finally, it should be noted that in the meantime of the review process of the present study, an analysis of pitch angle scattering at the dayside magnetopause with the very high resolution measurements of the Magnetospheric Multiscale mission was published by *Lavraud et al*. [2016]; their results largely confirm these earlier Cluster observations.

Acknowledgments
We acknowledge the Cluster instrument teams. The Cluster data were obtained from the Cluster Science Archive (http://www.cosmos.esa.int/web/csa). This work was supported by the National Natural Science Foundation of China (grants 41574163 and 41231066) and the Specialized Research Fund for State Key Laboratories. This work was completed while Y.C. Zhang, selected by China Scholarship Council, was visiting IRAP/CNRS as a visiting scholar awarded under the State Scholarship Fund (201404910001). A. Fazakerley and Z. Yao gratefully acknowledge support from the UK Science and Technology Facilities Council grant ST/K000977/1, while B. Mihaljcic acknowledges support from ESA CSA.

References

Baker, D. N., S. J. Bame, W. C. Feldman, J. T. Gosling, R. D. Zwickl, J. A. Slavin, and E. J. Smith (1986), Strong electron bidirectional anisotropies in the distant tail: ISEE 3 observations of polar rain, *J. Geophys. Res.*, *91*, 5637–5662, doi:10.1029/JA091iA05p05637.

Balogh, A., et al. (2001), The Cluster Magnetic Field investigation: Overview of in-flight performance and initial results, *Ann. Geophys.*, *19*, 1207–1217.

Bessho, N., and A. Bhattacharjee (2005), Collisionless reconnection in an electron-positron plasma, *Phys. Rev. Lett.*, *95*(24), 245001, doi:10.1103/PhysRevLett.95.245001.

Bessho, N., L.-J. Chen, K. Germaschewski, and A. Bhattacharjee (2015), Electron acceleration by parallel and perpendicular electric fields during magnetic reconnection without guide field, *J. Geophys. Res. Space Physics*, *120*, 9355–9367, doi:10.1002/2015JA021548.

Borg, A. L., M. Øieroset, T. D. Phan, F. S. Mozer, A. Pedersen, C. Mouikis, J. P. McFadden, C. Twitty, A. Balogh, and H. Re'me (2005), Cluster encounter of a magnetic reconnection diffusion region in the near-Earth magnetotail on September 19, 2003, *Geophys. Res. Lett.*, *32*, L19105, doi:10.1029/2005GL023794.

Büchner, J., and L. M. Zelenyi (1989), Regular and chaotic charged particle motion in magnetotaillike field reversals: 1. Basic theory of trapped motion, *J. Geophys. Res.*, *94*, 11,821–11,842, doi:10.1029/JA094iA09p11821.

Chaston, C. C., et al. (2009), Kinetic Alfvén wave turbulence and transport through a reconnection diffusion region, *Phys. Rev. Lett.*, *102*, 015,001.

Chen, J. (1992), Nonlinear dynamics of charged particles in the magnetotail, *J. Geophys. Res.*, *97*, 15,011–15,050, doi:10.1029/92JA00955.

Dunlop, M. W., Q.-H. Zhang, C.-J. Xiao, J.-S. He, Z. Pu, R. C. Fear, C. Shen, and C. P. Escoubet (2009), Reconnection at high latitudes: Antiparallel merging, *Phys. Rev. Lett.*, *102*, 075,005, doi:10.1103/PhysRevLett.102.075005.

Eastwood, J. P., T.-D. Phan, F. S. Mozer, M. A. Shay, M. Fujimoto, A. Retinò, M. Hesse, A. Balogh, E. A. Lucek, and I. Dandouras (2007), Multi-point observations of the Hall electromagnetic field and secondary island formation during magnetic reconnection, *J. Geophys. Res.*, *112*, A06235, doi:10.1029/2006JA012158.

Fazakerley, A., et al. (2010), Cluster-PEACE in-flight calibration status, in *The Cluster Active Archive*, edited by H. Laakso et al., 281 pp., Springer, Netherlands.

Huang, S. Y., M. Zhou, F. Sahraoui, X. H. Deng, Y. Pang, Z. G. Yuan, Q. Wei, J. F. Wang, and X. M. Zhou (2010), Wave properties in the magnetic reconnection diffusion region with high b: Application of the k-filtering method to Cluster multispacecraft data, *J. Geophys. Res.*, *115*, A12211, doi:10.1029/2010JA015335.

Johnstone, A. D., et al. (1997), Peace: A plasma electron and current experiment, *Space Sci. Rev.*, *79*, 351–398.

Laakso, H., C. Perry, S. McCaffrey, D. Herment, A. J. Allen, C. C. Harvey, C. P. Escoubet, C. Gruenberger, M. G. G. T. Taylor, and R. Turner (2010), Cluster active archive: Overview, in *The Cluster Active Archive*, edited by H. Laakso et al., pp. 3–37, Springer, Netherlands.

Lavraud, B., et al. (2016), Currents and associated electron scattering and bouncing near the diffusion region at Earth's magnetopause, *Geophys. Res. Lett.*, *43*, 3042–3050, doi:10.1002/2016GL068359.

Ma, Z. W., and A. Bhattacharjee (2001), Hall magnetohydrodynamic reconnection: The Geospace Environment Modeling challenge, *J. Geophys. Res.*, *106*, 3773–3782, doi:10.1029/1999JA001004.

Northrop, T. G. (1963), Adiabatic charged-particle motion, *Rev. Geophys.*, *1*, 283, doi:10.1029/RG001i003p00283.

Paschmann, G. (2008), Recent in-situ observations of magnetic reconnection in near-Earth space, *Geophys. Res. Lett.*, *35*, L19109, doi:10.1029/2008GL035297.

Rème, H., et al. (2001), First multispacecraft ion measurements in and near the Earth's magnetosphere with the identical Cluster ion spectrometry (CIS) experiment, *Ann. Geophys.*, *19*, 1303–1354.

Rong, Z. J., W. X. Wan, C. Shen, X. Li, M. W. Dunlop, A. A. Petrukovich, T. L. Zhang, and E. Lucek (2011), Statistical survey on the magnetic structure in magnetotail current sheets, *J. Geophys. Res.*, *116*, A09218, doi:10.1029/2011JA016489.

Schwartz, S. J. (1998), Shock and discontinuity normals, Mach numbers and related parameters, in *Analysis Methods for Multi-spacecraft Data*, edited by G. Paschmann and P. W. Daly, pp. 249–270, Int. Space Sci. Inst., Bern.

Sergeev, V. A., E. M. Sazhina, N. A. Tsyganenko, J. A. Lundblad, and F. Soraas (1983), Pitch-angle scattering of energetic protons in the magnetotail current sheet as the dominant source of their isotropic precipitation into the ionosphere, *Planet. Space Sci.*, *31*, 1147.

Shen, C., X. Li, M. Dunlop, Z. X. Liu, A. Balogh, D. N. Baker, M. Hapgood, and X. Wang (2003), Analyses on the geometrical structure of magnetic field in the current sheet based on cluster measurements, *J. Geophys. Res.*, *108*(A5), 1168, doi:10.1029/2002JA009612.

Shen, C., X. Li, M. Dunlop, Q. Q. Shi, Z. X. Liu, E. Lucek, and Z. Q. Chen (2007), Magnetic field rotation analysis and the applications, *J. Geophys. Res.*, *112*, A06211, doi:10.1029/2005JA011584.

Shen, C., et al. (2008), Flattened current sheet and its evolution in substorms, *J. Geophys. Res.*, *113*, A07S21, doi:10.1029/2007JA012812.

Shen, C., et al. (2014), Direct calculation of the ring current distribution and magnetic structure seen by Cluster during geomagnetic storms, *J. Geophys. Res. Space Physics*, *119*, 2458–2465, doi:10.1002/2013JA019460.

Wang, R., Q. Lu, C. Huang, and S. Wang (2010), Multispacecraft observation of electron pitch angle distributions in magnetotail reconnection, *J. Geophys. Res.*, *115*, A01209, doi:10.1029/2009JA014553.

Wang, X., A. Bhattacharjee, and Z. W. Ma (2001), Scaling of collisionless forced reconnection, *Phys. Rev. Lett.*, *87*, 265,003.

Xiao, C. J., et al. (2007), A Cluster measurement of fast magnetic reconnection in the magnetotail, *Geophys. Res. Lett.*, *34*, L01101, doi:10.1029/2006GL028006.

Yang, Y. Y., C. Shen, Y. C. Zhang, Z. J. Rong, X. Li, M. Dunlop, Y. H. Ma, Z. X. Liu, C. M. Carr, and H. Rème (2014), The force-free configuration of flux ropes in geomagnetotail: Cluster observations, *J. Geophys. Res Space Phys.*, *119*, 6327–6341, doi:10.1002/2013JA019642.

Young, S. L., R. E. Denton, B. J. Anderson, and M. K. Hudson (2008), Magnetic field line curvature induced pitch angle diffusion in the inner magnetosphere, *J. Geophys. Res.*, *113*, A03210, doi:10.1029/2006JA012133.

Zhang, Y. C., et al. (2013), Two different types of plasmoids in the plasma sheet: Cluster multisatellite analysis application, *J. Geophys. Res. Space Physics*, *118*, 5437–5444, doi:10.1002/jgra.50542.

Zhou, M., et al. (2009), Observation of waves near lower hybrid frequency in the reconnection region with thin current sheet, *J. Geophys. Res.*, *114*, A02216, doi:10.1029/2008JA013427.

Zou, H., Q.-G. Zong, G. K. Parks, Z. Pu, H.-F. Chen, and L. Xie (2011), Response of high-energy protons of the inner radiation belt to large magnetic storms, *J. Geophys. Res.*, doi:10.1029/2011JA016733.